J Digit Imaging (2012) 25:307–317
DOI 10.1007/s10278-011-9433-7

Computer-Based Route-Definition System for Peripheral Bronchoscopy

Michael W. Graham · Jason D. Gibbs · William E. Higgins

Published online: 15 November 2011

Abstract Multi-detector computed tomography (MDCT) scanners produce high-resolution images of the chest. Given a patient's MDCT scan, a physician can use an image-guided intervention system to first plan and later perform bronchoscopy to diagnostic sites situated deep in the lung periphery. An accurate definition of complete routes through the airway tree leading to the diagnostic sites, however, is vital for avoiding navigation errors during image-guided bronchoscopy. We present a system for the robust definition of complete airway routes suitable for image-guided bronchoscopy. The system incorporates both automatic and semiautomatic MDCT analysis methods for this purpose. Using an intuitive graphical user interface, the user invokes automatic analysis on a patient's MDCT scan to produce a series of preliminary routes. Next, the user visually inspects each route and quickly corrects the observed route defects using the built-in semiautomatic methods. Application of the system to a human study for the planning and guidance of peripheral bronchoscopy demonstrates the efficacy of the system.

Keywords 3D pulmonary imaging · Procedure planning · Image-guided intervention · Bronchoscopy · Lung cancer · MDCT · Virtual bronchoscopic navigation · Route planning

M. W. Graham · J. D. Gibbs · W. E. Higgins (✉)
Department of Electrical Engineering, Penn State University,
University Park,
Pennsylvania, PA 16802, USA
e-mail: weh2@psu.edu
URL: http://www.mipl.ee.psu.edu

M. W. Graham
Google, Inc.,
Pittsburgh, PA 15213, USA

J. D. Gibbs
Broncus Technologies, Inc., State College,
Broncus, PA 16801, USA

Introduction

Current multi-detector computed tomography (MDCT) scanners are able to produce 3D chest scans having voxel resolution on the order of 0.5 mm [1, 2]. Such scans enable the definition and visualization of small airways deep in the lung periphery. In addition, ultrathin bronchoscopes having diameters approaching 2 mm permit deep navigation into the airway tree, making minimally invasive peripheral lung procedures feasible [3, 4]. Transthoracic needle aspiration has remained the prime method for peripheral nodule biopsy, but entails a significant risk of pneumothorax, cannot be applied to many suspect nodules, and can result in other complications such as malignant seeding along the needle track [5, 6]. Hence, considerable recent research has focused on using bronchoscopy for peripheral nodule biopsy [3, 4, 7]. Unfortunately, it has long been known that physicians vary considerably in their ability to navigate a bronchoscope correctly to peripheral diagnostic sites [8, 9].

Note that before bronchoscopy, a physician first preplans a suitable 3D airway route leading to a region of interest (ROI) by mentally examining the stack of 2D sections constituting a patient's 3D chest scan. Physicians, however, begin making errors in identifying airways at bronchial generation 2 (trachea=bronchial generation 1), with route planning performance deteriorating to 40% by bronchial generation 4 [10, 11]. This poor performance in mental procedure planning directly impacts performance during later bronchoscopy. A recent study demonstrated that 14 bronchoscopists could navigate successfully to only 31% of ROIs situated six to eight bronchial generations into the lungs [9]. Thus, it is well recognized that some form of image-based route planning prior to a procedure is imperative [12, 13].

The modern approach to peripheral bronchoscopy employs an image-guided intervention (IGI) system [4, 12, 14–16]. The use of an IGI system, however, also

requires initial route planning. Later, during live bronchoscopy, the IGI system uses the preplanned routes to help the physician navigate the bronchoscope to the desired ROIs. Unfortunately, as pointed out above, accurate route planning is challenging. Shinagawa et al. pointed out this difficulty in their seminal efforts in peripheral bronchoscopy [15]. In their studies, an expert radiologist manually defined the desired airway routes using a patient's MDCT chest scan. They reported no results reaching an airway branch at bronchial generation 8 and recommended the development of an efficient means for planning peripheral bronchoscopic procedures [12]. Schwarz et al. also relied on a tedious procedure planning approach [16]. More recent efforts introduced some automated image analysis into route planning, but still suffered from drawbacks [13]. In this paper, we describe a computer-based airway route-definition system suited to the demands of peripheral bronchoscopy.

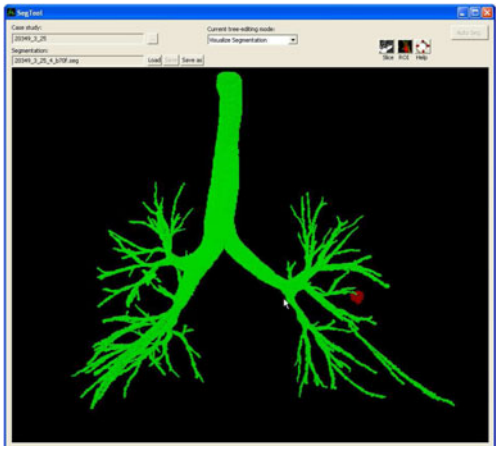

Fig. 1 Top-level graphical user interface (*GUI*) for the proposed route-definition system. The user interacts with the system's tools and interactive views through the GUI to inspect candidate routes and arrive at final route suitable for bronchoscopy. The view shown in the main display panel depicts the raw segmentation (*green*) and a predefined ROI (*red*) for case 25. Figures 2 and 3 illustrate other views that can appear in the GUI's display panel

Methods

The proposed airway route-definition system constitutes part of a large IGI suite we have been developing for the planning and guidance of bronchoscopy [9, 17–20]. Use of the complete IGI suite involves the following major stages: (a) procedure planning; (b) procedure preview; and (c) live image-guided bronchoscopy. The system described in this paper focuses on procedure planning. Companion works discuss procedure preview, which involves a virtual rehearsal of the procedure plan [18, 20], and image-guided bronchoscopy, which entails performing the desired bronchoscopy under guidance from the plan [9, 17, 19]. "Results" also illustrates the use of a plan for image-guided bronchoscopy.

Focusing on procedure planning, the airway route-definition system draws upon automatic and semiautomatic 3D image analysis, along with a set of user-friendly graphical tools, to enable the definition of complete airway routes. The system runs on a standard Windows 7 PC and consists of software built using Visual Studio 2008, Visual C++, and OpenGL [21]. Figure 1 illustrates the top-level graphical user interface (GUI) for the route-definition system.

The system accepts as inputs a patient's 3D MDCT chest scan and predefined diagnostically important ROIs. We assume that the input MDCT scan has voxel resolution approximately on the order of 1 mm. Airway lumens generally appear dark in MDCT, having HU values near −1,000 HU, while airway walls and other surrounding soft tissue structures and ROIs appear brighter with HU values greater than −200 [22, 23]. As is well established in practice, these nominal HU ranges offer considerable flexibility in extracting the airways necessary for route-definition. For our studies, we employed the semiautomatic live wire to predefine ROIs in the input MDCT scan [24].

The user interacts with the system through the system GUI and its built-in set of integrated tools. Given the inputs, the user employs the system in three steps:

1. Three-dimensional airway tree definition
2. Preliminary route computation
3. Route inspection and completion

Three-dimensional airway tree definition (step 1) extracts the 3D airway tree and defines the airway endoluminal surfaces from the 3D MDCT scan. This entails an automatic method that includes four operations. To begin, a region-growing technique defines a conservative airway tree segmentation. The next three operations focus on adding missing peripheral airways to the conservative segmentation. The first operation exhaustively locates candidate 2D cross-sections of missing airways. Next, using a graph structure that captures the properties of potential connections between the cross-sections, an optimal search identifies and constructs candidate airway segments consisting of contiguous cross-sections. Finally, an optimal search of a directed graph, which captures the potential spatial relationships and connections between the candidate segments, produces the final peripheral airways to add to the conservation airway tree segmentation. This completes the definition of the 3D airway tree. Graham et al. [19] gave complete method detail.

Given the defined 3D airway tree, preliminary route computation (step 2) automatically computes candidate airway routes leading to each ROI. To do this, a method, which draws upon concepts from 3D differential geometry, first performs a sub-voxel-level topographic analysis of the

3D airway tree's interior surface to define a set of airway central axes and bifurcations specifying the airway tree's complete centerline structure. Next, for each ROI, an optimization method locates a route traversing the airway tree centerline structure that is: (1) closest to the ROI and (2) enables the bronchoscope to fit through all points along the route toward the ROI. Constraint (2) simultaneously takes into account the diameter and bending properties of the bronchoscope along with the diameters of the traversed airways. Gibbs et al. [18] gave a complete description of these operations. Figure 2 gives example outputs for steps 1 and 2. As elaborated on further below, the operations of these two steps also initialize important data structures related to the defined airway tree and computed routes.

Note that partial volume effects, noise, and image reconstruction artifacts can limit the effectiveness of 3D airway tree definition in producing the full complement of small airways necessary for defining a complete airway route leading to a peripheral ROI. We define a complete airway route as the collection of all airways either navigated or perceived during bronchoscopy along a route to a given ROI. We point out that existing 3D airway tree definition methods segment virtually 100% of airways to bronchial generation 3 (segmental level), but tend to exhibit segmentation rates ranging as low as 32% for more peripheral airways beyond bronchial generation 3 (sub-segmental level and beyond) [19]. The 3D airway tree definition method we use often extracts two to three more generations of airway branches than several other known methods, but the method still can miss small-diameter airways that exhibit weak image signatures or appear disconnected from the airway tree [19, 23, 25–28]. Thus, after completing the automatic operations of steps 1 and 2, the routes associated with each ROI are preliminary, and further processing is needed.

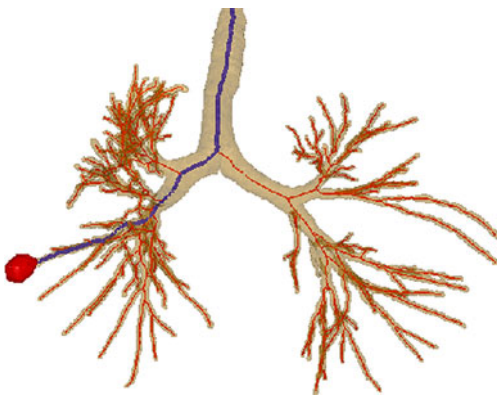

Fig. 2 Example outputs from 3D airway tree definition and preliminary route computation for case 24 (scan dimensions, 512×512×608; voxel dimensions, $\Delta x=\Delta y=0.62$ mm, $\Delta z=0.5$ mm; MDCT scanner, Siemens Sensation-16). The surface rendering depicts the defined airway tree (*brown*) and airway centerlines (*red*), in addition to a preliminary route (*blue*) to a suspect peripheral nodule (*red*). For this case, the set of airway centerline branches B consisted of $M=315$ distinct branches $\{b_1,\ldots,b_M\}$, while the set of routes R contained only one route r_1 as only one ROI was defined. Route r_1 consisted of 13 contiguous branches $b_j \in B$, starting with the trachea b_1

Returning to our system, two types of airways constituting a complete airway route may be missing in the preliminary routes:

1. Final terminating airways leading to an ROI
2. Important child airways encountered along a route

Missing a route's terminating airway obviously means that the IGI system will not be able to provide sufficient guidance to reach the ROI during bronchoscopic navigation. Also, as an option, the user may wish to extend the end of a route to provide a better angle for viewing and/or biopsying an ROI.

The impact of missing child airways introduces a more subtle problem. Note that all IGI systems for bronchoscopy use some form of virtual bronchoscopy (VB) [4, 9, 12–16, 29, 30]. During bronchoscopy, the IGI system guides the physician to an ROI by presenting a sequence of MDCT-derived VB views of airways encountered along the preplanned route. Each VB view, also referred to as an endoluminal rendering, is an MDCT-based graphical depiction of the airway tree's internal (endoluminal) surface at a specific viewing site along the route. Because the VB views along the route strongly resemble the bronchoscopic video stream along the same route during live bronchoscopy, they have been proven to be an indispensable aid for bronchoscopic navigation.

During bronchoscopic navigation, VB views of airway bifurcation points serve as the essential vital landmarks because they indicate to the physician when to turn the bronchoscope. To guarantee correct VB views of bifurcations along an entire route, the defined 3D airway tree must capture all airways perceived during bronchoscopy along a route, including those not navigated. If any side child airway constituting part of a bifurcation along the route is missed, then the VB view presented by the IGI system near the miss will mislead the physician, resulting in navigation errors (e.g., Fig. 6).

Therefore, to arrive at final complete routes, the user must invoke step 3, route inspection and completion. This step involves a series of semiautomatic and interactive operations applied to each ROI's preliminary route. Route inspection and completion involves two major operations: (1) route inspection and (2) defect correction.

To perform the operations of route inspection and completion, the user interacts with the airway tree segmentation and MDCT scan through the system's GUI. In particular, the user interacts with a fused view incorporating the 3D airway tree and a 2D oblique cross-section (Fig. 3a). The oblique cross-section is a small local 2D planar image through the 3D MDCT scan situated orthogonal to the current viewing site

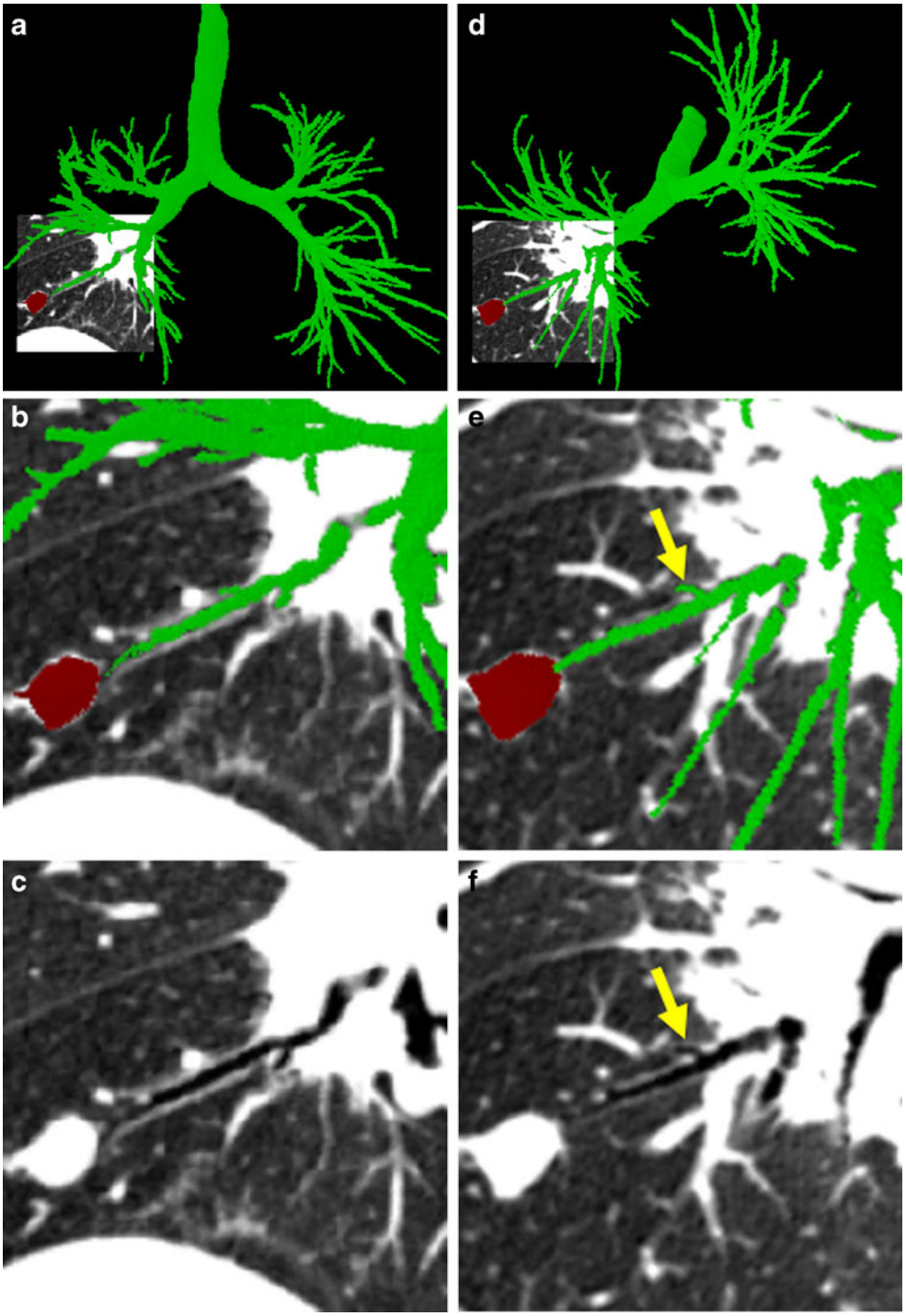

Fig. 3 Illustration of system GUI interaction and route inspection (case 24). **a** The global 3D airway tree (*green*) fused with the local oblique cross-section view. The ROI, a suspect cancer nodule situated in the right lower lobe, appears in *red*. The oblique cross-section shown here and in other figures has isotropic pixel resolution 0.5 mm and uses display window [−1,000 HU, −200 HU]. **b** A close-up of the oblique cross-section near the ROI. **c** The same oblique cross-section as (**b**) displayed without the airway tree or ROI. **d** Another fused view after rotating the 3D scene to give another view of the small peripheral airway of (**a**–**c**). This airway is marked by *yellow arrows* in (**e**) and (**f**)

along the route of interest. During route inspection, the user views a movie of the oblique cross-sections along an ROI's preliminary route and observes the route's completeness. This allows the user to quickly scan the segmented tree, verify the automatically extracted airways, and locate small missed airways (Fig. 3b, c). During this viewing procedure, the user can freely rotate or pan the complete fused view or the local 2D oblique view in 3D space (Fig. 3d). The user can also select zoom level, change the display intensity window, and scroll through oblique cross-sections manually. In addition, during interaction, the airway tree and a small navigation compass globally orient the user along the route, while the oblique cross-section depicts local airway/lung structure. Figure 3 illustrates system GUI interaction during route inspection.

All preliminary routes must be inspected to verify the completeness of a route and to identify defects. Note that a typical bronchoscopy virtually never involves more than

four ROIs. Thus, at most, four airway routes need be inspected, and, very importantly, an exhaustive definition of the airway tree is unnecessary. We point out, however, that final routes only include airway branches necessary for navigating to a given ROI.

If a route defect is detected during route inspection, the user can correct the defect through two semiautomatic methods constituting defect correction: (1) airway tree augmentation and (2) branch addition. To facilitate defect correction, the system draws upon three data structures computed during the automatic analysis of steps 1 and 2:

1. A candidate airway segment list $\mathbf{S} = \{S_i,\ i = 1, \ldots, N_S\}$, where *Si* denotes the *i*th candidate airway segment and N_S denotes the total number of candidate segments.
2. A directed graph *T* representing the defined airway tree and other potential airway candidates.
3. Structures **B** and **R** representing the airway centerline branches and preliminary ROI routes. We use the notation of Graham et al. [19] for the airway segments *Si* and graph *T*.

A candidate airway segment S_i corresponds to a portion of a possible airway constituting the airway tree. The vertices of directed graph *T* equal the segments $Si \in \mathbf{S}$, while the edges of *T* denote connections between segments. For example, graph edge $(i,\ P(i))$ signifies that a connection exists between segment *Si* and a parent segment $S_{P(i)}$. The analysis of step 1 predetermines the optimal parent segment $S_{P(i)}$ for each segment $Si \in \mathbf{S}$, computes an image-based connection between *Si* and $S_{P(i)}$, and assigns a cost to the connection. It also produces the defined airway tree, represented as a partition T_f of the complete graph *T*, i.e., T_f onsists of the connected subset of vertices (airway segments) and edges (connections) in *T* constituting the defined airway tree. To facilitate defect correction, the system, however, also retains the complete graph *T*, including the vertices and edges rejected for T_f.

Regarding **B** and **R**, **B**=set of airway centerline branches $\{\mathbf{b}_1, \ldots, \mathbf{b}_M\}$ and **R**=set of preliminary airway routes $\{\mathbf{r}1, \ldots, \mathbf{r}N\}$. Each of the *M* centerline branches $\mathbf{b}j \in \mathbf{B}$ corresponds to a distinct airway, with **b**1 corresponding to the trachea at bronchial generation 1. Each of the *N* routes $\mathbf{r}_k \in \mathbf{R}$ in turn consists of an ordered connected sequence of

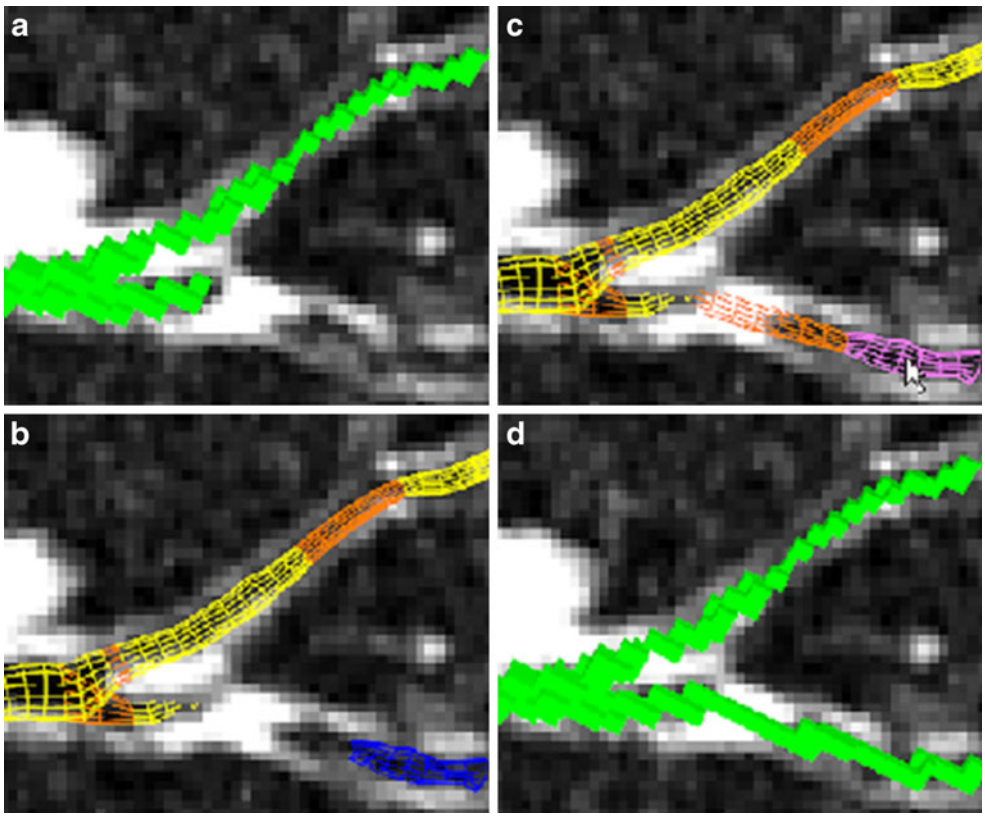

Fig. 4 Example of airway tree augmentation for case 25 (scan dimensions, 512×512×796; voxel dimensions, $\Delta x = \Delta y = 0.86$ mm, $\Delta z = 0.50$ mm; MDCT scanner, Siemens Sensation-16). **a** Current voxel-based local oblique cross-section view of the defined airway tree T_f before defect correction. **b** Wire frame surface representation of branch segments (*yellow*) and branch segment connections (*orange*) belonging to T_f and a branch segment (*blue*) not currently constituting part of the defined tree T_f. This view clearly indicates a missing branch defect. The disconnected branch segment $S_i \notin S$ disconnects from the main defined airway tree because of a layer of high-intensity voxels and appears to have no visible child branches. **c** By selecting the missed branch segment, the user enables the segment S_i and its previously computed and stored parent connection $(i,P(i))$ to be added to the defined tree T_f. **d** Voxel form of the resulting augmented airway tree segmentation

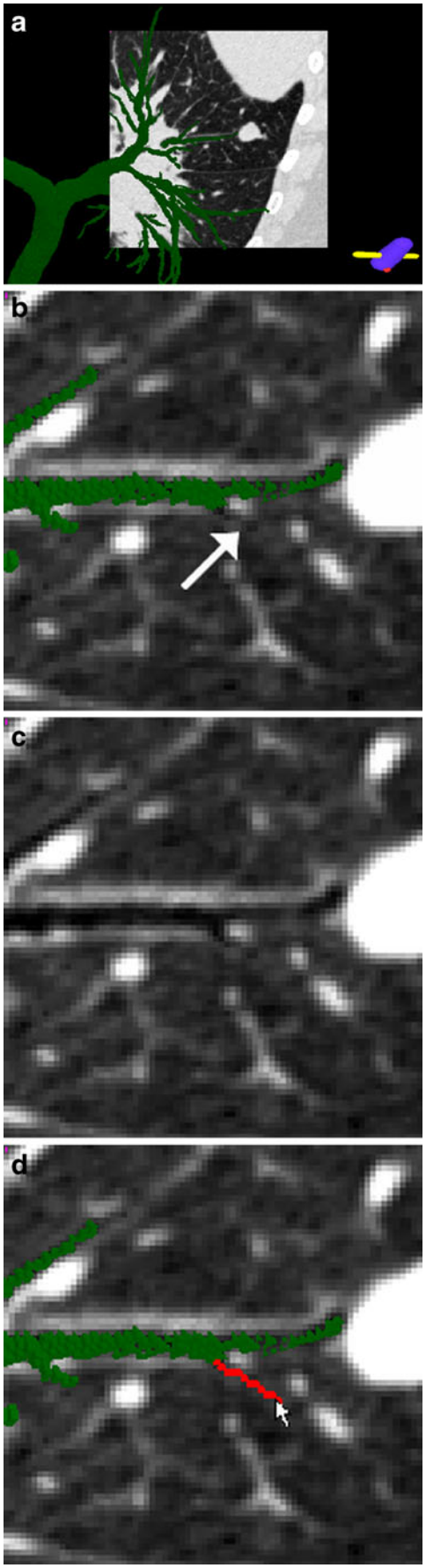

◀ **Fig. 5** An illustration of branch addition (case 24). **a** Fused system view in the vicinity of a missing airway. **b**, **c** Close-up views in the vicinity of the missing branch, both with (**b**) and without (**c**) the airway tree segmentation. The *arrow* in (**b**) highlights the airway missed by automatic 3D airway tree definition and T_f. **d** Branch Addition adds a small child airway $b_j \notin B$ (*red*) to T_f

branches in **B** necessary to reach a particular ROI from the trachea. Note that the term "bronchial generation" refers to the number of bronchial branches constituting a route; this follows other recent works in image-guided bronchoscopy [9, 12–15]. As stated earlier, the airway bifurcation points are the essential landmarks needed by the bronchoscopist during navigation, and these are the points that terminate each bronchial generation. Figure 2 depicts examples of **B** and **R** for a particular patient scan.

Given these data structures, the two methods for defection correction are as follows. Airway tree augmentation provides a simple interactive function for augmenting the existing defined airway tree, T_f, with airway branches previously rejected by step 1. Such branches generally have substantial support within the MDCT scan, but appear separated from the main airway tree because of scan imperfections or an airway stenosis or blockage. To apply the method, the user focuses the oblique cross-section over the vicinity of the observed defect and then clicks the mouse anywhere within the missing airway. If a corresponding segment(s) $Si \in \mathbf{S}$ exists at this location, then Si and its associated precomputed connection (i, P (i)) are added to the 3D airway tree T_f. In addition, the airway tree endoluminal surface data are augmented to include this new region. Finally, if the added airway is a terminating airway leading an ROI, then the corresponding airway route $\mathbf{r}_k$ is updated accordingly with a new centerline branch $\mathbf{b}j \notin \mathbf{B}$ corresponding to the new airway. Figure 4 illustrates airway tree augmentation.

Certain very weakly supported airways on the order of 1 voxel thick will not be represented in the precomputed graph T and segment set S. Branch addition assists in the task of adding such airways via a method based on the semiautomatic live wire [24, 31]. To perform branch addition, the user again positions the oblique cross-section over the missed branch and then selects a seed point inside the currently available segmented airway tree. Next, the user hovers the mouse cursor over a point along the missing airway. The system's actively running live wire engine then automatically computes and displays in real time the optimal 2D path from the seed point to the cursor location on the cross-section. The optimization method uses an automatic graph search algorithm driven by the local cost function $l(p, r)$ [24]

$$l(p,r) = w_G f_G(r) + w_Z f_Z(r) + w_{D1} f_{D1}(p,r) + w_{D2} f_{D2}(p,r),$$

where $r \in N(p)$, $N(p)$ equals the set of eight neighbors of seed point p, $f_Z(r)$ and $f_G(r)$ are costs measuring local intensity

gradient variation, $f_{D1}(p,r)$ and $f_{D2}(p,r)$ are costs influenced by local intensity gradient direction, and w_G through w_{D2} are user-specified weights.

If the displayed path is acceptable, the user clicks the mouse at the cursor location to save the path. This path endpoint then becomes a new seed point p, and the user repeats the process until the desired branch is defined. Our system's version of the live wire for branch addition favors a path that travels the shortest distance between the two points while also favoring low-intensity air-like regions. As a branch may not lie entirely within any single oblique cross-section, the user can freely rotate the cross-section or the entire 3D scene at any time to obtain a more suitable view during branch addition.

After branch addition, the 3D airway tree is again updated, as is the corresponding endoluminal surface data and segmentation. Also, if the added airway terminates a route leading to an ROI, then the involved route $\mathbf{r}_k$ is also updated with an additional centerline branch $\mathbf{b}j \notin \mathbf{B}$ corresponding to the new airway. Figure 5 demonstrates branch addition.

Finally, we briefly point out that our system also provides a method for semi-automatically deleting individual airway branches or entire sub-trees of the segmented airway tree [32]. Similar to airway tree augmentation, the user interactively selects the undesired airway. The system then automatically updates T_f y deleting the unwanted airway and any connected sub-tree. This capability addresses the well-known problem that automatic airway tree segmentation methods may be prone to defining extraneous false "airways" or sub-trees arising because of leakages into the lung parenchyma, e.g., Fig. 3 in [19] and Fig. 7 in [23]. We never used this capability, however, for any ROI considered in our peripheral human study described in the next section [33]. This may have occurred because we observed in a ground-truth study that our 3D airway tree segmentation method

Table 1 Summary route-definition results using the proposed system for a human peripheral bronchoscopy study. Cases are numbered according to an IRB Protocol (the study began with case 24. Missing cases, such as 31, involve consented patients for whom no data was collected). Route length=total number of bronchial generations, starting from the trachea traversed by an ROI route. Missed airways added to a route during defect correction are listed by bronchial generation number for airway tree augmentation and branch addition; "none" indicates that a route had no observed defects. The two distinct RUL routes for case 38 exhibited the same defects, making defect correction efficient. These two routes terminated at different generation 8 locations. *LUL* left upper lobe, *LLL* left lower lobe, *RUL* right upper lobe

Case no.	ROI location	Route length	Airway tree augmentation	Branch addition	Total defects
24	RLL	13	None	8,12	2
25	LUL	8	None	7	1
26	LUL	8	8	None	1
	RUL	8	8	None	1
28	RUL	9	None	None	0
	LUL	12	None	11	1
29	LUL-1	4	None	None	0
	LUL-2	13	10,11,12,13	9,10,11,12	8
30	RLL	11	None	8,9	3
33	RUL	13	13	10,12	3
	RLL	10	8,9,10	8,9	5
	LLL	12	None	9,10	2
34	LUL	9	9	7	2
	RML	7	None	None	0
35	RML	7	7	6	2
	RUL	7	None	None	0
	LUL	7	None	None	0
37	RUL	7	7	6	2
	RUL	4	None	None	0
38	RUL-1	8	5,6,7,8	6,7	6
	RUL-2	8	5,6,7,8	6,7	6
	LUL	13	None	10,12	2
39	RLL	5	None	None	0
	LLL	7	None	None	0
40	RML-1	4	None	None	0
	RML-2	4	None	None	0
41	RLL-1	13	None	11,12	2
	RLL-2	12	None	10	1
	RUL	8	None	None	0
42	RUL-1	8	None	None	0
	RUL-2	9	None	6	1

only produced two erroneous branches over a total of 1,112 airways [19]. Nevertheless, we believe it is important to have a false-branch deletion capability as false branches can create misleading false bifurcations [32].

Results

We applied the proposed system to an IRB-approved human study that tested our complete IGI system for planning and guiding peripheral bronchoscopy (Penn State IRB protocol #20349-3) [33]. The 3D MDCT patient scans were generated using either a Siemens Sensation-16, Emotion-40, or Definition-64 MDCT scanner using a standard scanning protocol for lung cancer patients, i.e., during a scan, a patient performed a full-inspiration breath hold of ≤20 s to reduce lung motion artifacts. Scan parameters were as follows: voltage 120 kVp and tube current range 174–540 mA s or voltage 130 kVp and tube current range 138–237 mA s. The final 3D scans were reconstructed using either a B31, B41, or B50 kernel and consisted of a series of 0.75-mm-thick axial plane sections spaced 0.5 mm apart. Axial plane resolution $\Delta x=\Delta y$ ranged from 0.52 to 0.92 mm.

Table 1 summarizes the route-definition results. For 15 cases, the physician predefined a total of 31 peripheral ROIs. The system automatically computed 31 preliminary ROI routes, with the number of ROIs considered per case ranging between 1 and 3 (median, 2 ROIs). The number of bronchial generations traversed by the routes ranged between 4 and 13 (median, 8 generations).

Interactive route inspection revealed that 12 ROI routes (39%) had no defects, 2 routes (6%) only required airway tree augmentation, 9 routes (29%) only required branch addition, and 8 routes (26%) required both forms of defect correction. As the automatically computed preliminary routes were largely complete in all cases, it proved straightforward to correct the observed defects. The number of defects per case ranged between 0 and 8 (median=1). The mean bronchial generation number of a missing airway was 8.8, with no airway added before generation 5. Thus, all added branches

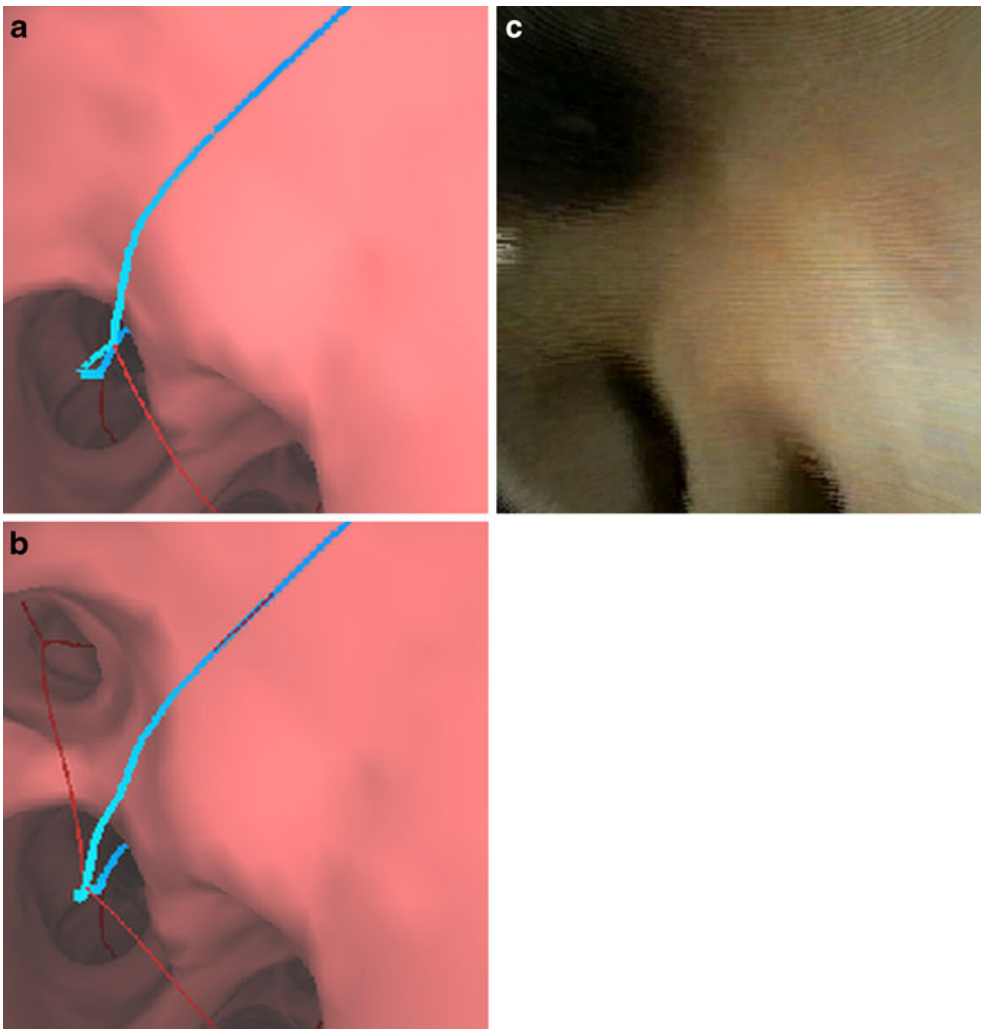

Fig. 6 Illustration of the necessity for branch addition (case 24). **a** Endoluminal rendering at a view site near a bronchial generation 8 airway along the route (*blue line*). **b** Same view as (**a**) after applying branch addition to add a missing thin child airway; note the new added centerline for this branch (*red line*). **c** A video frame captured with a 2.8-mm Olympus XP160F ultrathin bronchoscope during live image-guided bronchoscopy to the same site as (**a**, **b**) confirms the need for the additional branch

were located deep in the periphery. Missed branches occurred in all lung lobes and exhibited a diameter <3 mm.

Although the results of Table 1 indicate that the automatic analysis provided complete or nearly complete routes for all target ROIs, we emphasize that the peripheral branches added by the proposed system were vital for successful image-based bronchoscopic guidance. Case 20349-3-24 illustrates a striking example of how an added missed airway provided a vital landmark for proper bronchoscopic guidance (Fig. 6). The automatically segmented airway tree provided a route leading directly to the lesion (2), but missed two child branches incident upon the route at bronchial generations 8 and 12. The two branches were small, but dramatically affected virtual bronchoscopic views encountered along the route to the lesion. For example, Fig. 6 shows that the VB view at generation 8 before defect correction (Fig. 6a) erroneously missed an airway. After adding a missing branch, the correct VB view (Fig. 6b) now revealed a trifurcation instead of an incomplete bifurcation. A bronchoscopic video view captured during the live procedure (Fig. 6c) confirmed the correctness of the route (as described in [17, 18]; we use a well-established method for producing the VB views. As is well known in the realm of IGI systems for bronchoscopy, the very large HU difference between the airway lumen and walls makes VB view production robust [4, 14, 15].)

Finally, Fig. 7 illustrates the use of a complete airway route during live image guidance to a right lower lobe ROI (RLL-1 for case 41 in Table 1). The target ROI was successfully sampled by bronchoalveolar lavage. Overall, for the 15 cases of Table 1, we successfully collected biopsy samples for 90% of the ROIs (28/31), with no bronchoscope navigation errors attributable to the predefined routes. Retrospective analysis revealed that the three failures were situated at a bronchial generation ≥8 (case 33, RLL; case 34, LUL; and case 41, RUL). A study of the procedure videos revealed that these errors were preventable as the bronchoscopist clearly knew the correct branch to enter but did not maneuver the bronchoscope correctly. Higgins et al. [33] give complete study results.

Discussion

Image-based planning and guidance of peripheral bronchoscopy requires a robust knowledge of the peripheral airways visible during live bronchoscopy. This demands a system that enables the definition of complete airway routes in a patient's 3D MDCT scan before performing the procedure. Our proposed system draws upon a mix of automatic and semiautomatic image analysis methods to arrive at complete airway routes to peripheral ROIs. The system combines a set of computer graphics tools and judicious human interaction to facilitate the semiautomatic route correction techniques. The final complete endobronchial routes include both the airway

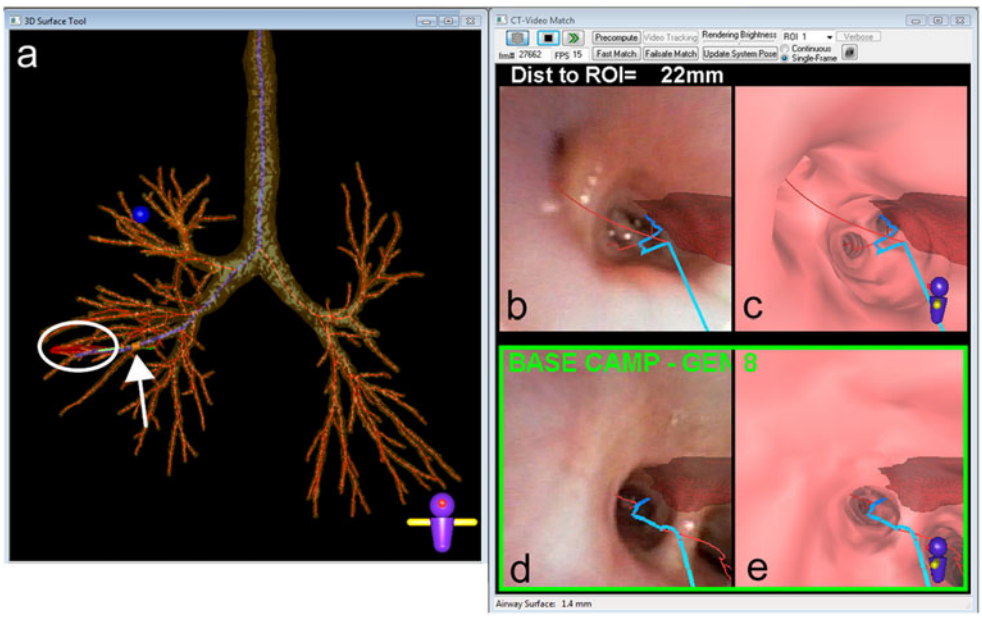

Fig. 7 View of IGI system during live guided bronchoscopy for case 41 [19, 33]. **a** Three-dimensional airway tree rendering depicts the the airway route used for guidance (*blue line*), airway centerlines (*red*), and the target ROI (*red*) highlighted by a *white oval*. The *yellow cylinder* indicated by the *white arrow* represents the current bronchoscope tip location at bronchial generation 9. **b** The live bronchoscopic video feed at the current bronchoscope location fused with the MDCT-derived guidance route (*blue*), airway centerlines (*red*), and ROI (*red*); the bronchoscope is 22 mm from the ROI, as indicated by the IGI system. **c** Corresponding VB view at the current bronchoscope location. **d**, **e** Saved "Base Camp" view of the fused video-MDCT view (**d**) and VB view (**e**) from the previous generation 8 airway along the route. Reference [19] gives more system detail

branches traversed by the bronchoscope during navigation to an ROI in addition to all visible child branches along the route. The system operates efficiently and fits smoothly into the standard clinical bronchoscopy workflow.

To enable successful route-definition to distant peripheral sites—i.e., sites deeper than five bronchial generations into the airway tree—the system requires 3D MDCT chest scans having a sub-millimeter resolution. We point out that this is in line with other recent studies using IGI systems for peripheral bronchoscopy [4, 9, 12, 14, 15]. Such scans are necessary for satisfactory definition of small peripheral airways ≤3 mm in diameter. Fortunately, current MDCT scanning protocols for lung cancer patients provide more than sufficient information for reconstructing high-resolution 3D scans. Hence, our requirement imposes no undue burden on the patient.

A trained technician carried out nearly all system tasks, with the physician's efforts limited to indicating target ROIs on the MDCT scan prior to route-definition. For a typical 3D MDCT chest scan, the automatic analysis of 3D airway tree definition and preliminary route computation required roughly 3 min of processing time, while route inspection and completion required under 7 min of interaction per ROI [18]. The system was a vital link in the subsequent stage of procedure preview [20]. We also applied the system successfully to a clinical study for image-guided peripheral bronchoscopy [33]. During this study, the physician was able to reach and successfully biopsy diagnostic sites at an unprecedented airway tree depth of 13 bronchial generations.

Acknowledgments This work was partially supported by NIH NCI grants R01-CA074325, R44-CA091534, and R01- CA151433. We would like to thank Drs. Rebecca Bascom, Muhammad Khan, and Syed Gilani of the Penn State Milton S. Hershey Medical Center for providing much of the data for the paper.

Conflict of interest statement William E. Higgins has an identified conflict of interest related to grant R01-CA151433, which is under management by Penn State and has been reported to the NIH.

References

1. Ueno J, Murase T, Yoneda K, Tsujikawa T, Sakiyama S, Kondoh K: Three-dimensional imaging of thoracic diseases with multi-detector row CT. J Med Invest 51(3–4):163–170, 2004
2. Dalrymple NC, Prasad SR, Freckleton MW, Chintapalli KN: Informatics in radiology (infoRAD): introduction to the language of three-dimensional imaging with multidetector CT. Radio- graphics 25(5):1409–1428, 2005
3. Haas A, Vachani A, Sterman D: Advances in diagnostic bronchoscopy. Am J Respiratory Critical Care Medicine 182 (5):589–597, 2010
4. Asano F: Virtual bronchoscopic navigation. Clin Chest Med 31 (1):75–85, 2010
5. Sawabata N, Ohta M, Maeda H: Fine-needle aspiration cytologic technique for lung cancer has a high potential of malignant cell spread through the tract. Chest 118(4):936–939, 2000
6. Yeow KM, Su IH, Pan KT, Tsay PK, Lui KW, Cheung YC, Chou AS: Risk factors of pneumothorax and bleeding: multivariate analysis of 660 CT-guided coaxial cutting needle lung biopsies. Chest 126:748–754, 2004
7. Chhajed PN, Tamm M: Bronchoscopy for small pulmonary nodules and mediastinal staging of lung cancer: just do it!". Am J Respir Crit Care Med 174(9):961–962, 2006
8. Minami H, Ando Y, Nomura F, Sakai S, Shimokata K: Interbronchoscopist variability in the diagnosis of lung cancer by flexible bronchoscopy. Chest 105(2):1658–1662, 1994
9. Merritt SA, Gibbs JD, Yu KC, Patel V, Rai L, Cornish DC, Bascom R, Higgins WE: Real-time image-guided bronchoscopy for peripheral lung lesions: a phantom study. Chest 134(5):1017–1026, 2008
10. Osborne D, Vock P, Godwin J, Silverman P: CT identification of bronchopulmonary segments: 50 normal subjects. AJR 142(1):47–52, 1984
11. Dolina MY, Cornish DC, Merritt SA, Rai L, Mahraj R, Higgins WE, Bascom R: Interbronchoscopist variability in endobronchial path selection: a simulation study. Chest 133(4):897–905, 2008
12. Shinagawa N, Yamazaki K, Onodera Y, Asahina H, Kikuchi E, Asano F, Miyasaka K, Nishimura M: Factors related to diagnostic sensitivity using an ultrathin bronchoscope under CT guidance. Chest 131(2):549–553, 2007
13. Asano F, Matsuno Y, Tsuzuku A, Anzai M, Shinagawa N, Moriya H, et al: Diagnosis of peripheral pulmonary lesions using a bronchoscope insertion guidance system combined with endobronchial ultrasonography with a guide sheath. Lung Cancer 60(3):366–373, 2008
14. Asano F, Matsuno Y, Shinagawa N, Yamazaki K, Suzuki T, Moriya H: A virtual bronchoscopic navigation system for pulmonary peripheral lesions. Chest 130(2):559–66, 2006
15. Shinagawa N, Yamazaki K, Onodera Y, Asano F, Nishimura M, et al: Virtual bronchoscopic navigation system shortens the examination time: feasibility study of virtual bronchoscopic navigation system. Lung Cancer 56(2):201–206, 2007
16. Schwarz Y, Greif J, Becker HD, Ernst A, Mehta A: Real-time electromagnetic navigation bronchoscopy to peripheral lung lesions using overlaid CT images: the first human study. Chest 129(4):988–994, 2006
17. Higgins WE, Helferty JP, Lu K, Merritt SA, Rai L, Yu KC: 3D CT–video fusion for image-guided bronchoscopy. Comput Med Imaging Graph 32(3):159–173, 2008
18. Gibbs JD, Graham MW, Higgins WE: 3D MDCT-based system for planning peripheral bronchoscopic procedures. Computers in Biology and Medicine 39(3):266–279, 2009
19. Graham MW, Gibbs JD, Cornish DC, Higgins WE: Robust 3D airway-tree segmentation for image-guided peripheral bronchoscopy. IEEE Trans Medical Imaging 29(4):982–997, 2010
20. Yu KC, Gibbs JD, Graham MW, Higgins WE: Image-based reporting for bronchoscopy. J Digital Imaging 23(1):39–50, 2010
21. Wright JRS, Lipchak B: OpenGL Superbible. Sams Publishing, Indianapolis, 2004
22. Kalender W: Computed Tomography: Fundamentals, System Technology, Image Quality, Applications. Publicis MCD Verlag, Munich, 2000
23. Kiraly AP, Hoffman EA, McLennan G, Higgins WE, Reinhardt JM: 3D human airway segmentation methods for clinical virtual bronchoscopy. Acad Radiol 9(10):1153–1168, 2002
24. Lu K, Higgins WE: Interactive segmentation based on the live wire for 3D CT chest image analysis. Int J Computer Assisted Radiol Surgery 2(3–4):151–167, 2007
25. Summers RM, Feng DH, Holland SM, Sneller MC, Shelhamer JH: Virtual bronchoscopy: segmentation method for real-time display. Radiology 200(3):857–862, 1996
26. Mori K, Hasegawa J, Suenaga Y, Toriwaki J: Automated anatomical labeling of the bronchial branch and its application

to the virtual bronchoscopy system. IEEE Trans Medical Imaging 19(2):103–114, 2000
27. Aykac D, Hoffman EA, McLennan G, Reinhardt JM: Segmentation and analysis of the human airway tree from three-dimensional X-ray CT images. IEEE Trans Med Imaging 22(8):940–950, 2003
28. Fetita C, Preteux F, Beigelman-Aubry C, Grenier P: Pulmonary airways: 3-D reconstruction from multislice CT and clinical investigation. IEEE Trans Med Imaging 23(11):1353–1364, 2004
29. Higgins WE, Ramaswamy K, Swift R, McLennan G, Hoffman EA: Virtual bronchoscopy for 3D pulmonary image assessment: state of the art and future needs. RadioGraphics 18(3):761–778, 1998
30. Haponik EF, Aquino SL, Vining DJ: Virtual bronchoscopy. Clinics in Chest Med 20(1):201–217, 1999
31. Mortensen EN, Barrett WA: Interactive segmentation with intelligent scissors. Graphical Models and Image Processing 60 (5):349–384, 1998
32. Graham MW, Gibbs JD, Higgins WE: Robust system for human airway tree segmentation. In: Pluim JPW, Reinhardt JM Eds. SPIE Medical Imaging 2008: Image Processing, Vol. 6914, 2008, pp. 69141J-1–69141J-18
33. Higgins W, Bascom R, Graham M, Gibbs J, Cornish D, Khan M: Image-guided bronchoscopic sampling of peripheral lesions: a human study. Am J Respir Crit Care Medicine 181:A5171, 2010